University of Science and Technology of Hanoi
UNDERGRADUATE SCHOOL

FINAL REPORT

BACHELOR GRADUATION

by

Nguyen Hoang Dang Khoa

Project:

EQUATION OF STATE OF NUCLEAR MATTER AND TIDAL DEFORMATION OF NEUTRON STAR

Supervisors: Prof.Dr. **Dao Tien Khoa**
Dr. **Ngo Hai Tan**

Jury:

Contents

Acknowledgement

First and foremost, I want to express my greatest thank to my main supervisor, Prof. Dao Tien Khoa for his supervision of my research study, who is the first person that has inspired me to pursue the path of a theoretical physicist back in my first year of undergraduate and also give me an opportunity to work with such an interesting topic regardless of my lack of background knowledge beforehand. Secondly, I would like to give my gratitude toward my secondary supervisor Dr. Ngo Hai Tan for helping me clearing various questions and misunderstanding, as well as supporting me with her broad knowledge in the field and encouraging me to work around on my own and get better with time. Without either of their supports, I would have never been able to get involved in active research this early, let alone finishing this work in the mean time. Beside, I am also deeply grateful to my family, lecturers and friends at USTH who never stop caring and cheerfully supporting me at any moment during my period of the final internship.

List of Abbreviations

APR	Akmal, Pandharipande and Ravenhall
BH	Black hole
BHF	Brueckner-Hartree-Fock
CFL	Confident level
EoS	Equation of States
GE	Gravito-electric
GEM	Gravitoelectromagnetism
GM	Gravito-magnetic
GR	General Relativity
GRB	Gamma-ray burst
GW	Gravitational wave
HF	Hartree-Fock
HI	Heavy-ion
MMC	Microscopic Monte Carlo
NM	Nuclear Matter
NN	Nucleon-Nucleon
NS	Neutron Star
PSR	Pulsar
TOV	Tolmann-Oppenheimer-Volkoff

List of Tables

List of Figures

Abstract

The equation of states of (EoS) of the spin polarized, asymmetric nuclear matter (NM) is studied within the nonrelativistic Hartree-Fock (HF) formalism using realistic choices for the in-medium (density dependent) nucleon-nucleon (NN) interaction, dubbed as CDM3Y4, CDM3Y5, CDM3Y6 and CDM3Y8. Two scenarios for the density dependence of the spin polarization Δ of baryons in NM are considered, and the obtained HF results are compared with the empirical constraints for the nuclear symmetry energy given by the nuclear structure studies and the astrophysical observations of the binary NS merger (GW170817 and GW190425). A partial spin polarization of baryons ($\Delta < 1.0$) at low baryon densities seems more reasonable, with the HF results for the symmetry energy and incompressibility of NM being quite close to the empirical values. The mean-field based EoS of asymmetric NM is used further to construct the β-stable neutron star (NS) matter of strongly interacting baryons (protons and neutrons), electrons, and muons.

The EoS of NS matter over a wide range of baryon densities is used as input for the calculation of the macroscopic configuration of NS within the framework of General Relativity (GR), like the gravitational mass M, radius R, gravito-electric and gravito-magnetic tidal deformability. Given the empirical constrains inferred from the gravitational-wave signals of GW170817 and the mass limit of the heaviest pulsars observed, we conclude that the EoS of NS matter given by the CDM3Y6 and CDM3Y8 versions of the in-medium NN interaction is the most appropriate for the study of NS. The Love numbers of the tidal deformation of NS in a binary system are calculated up to the 4^{th} order and a correlation of the tidal deformability of NS with its gravitational mass is shown.

Keywords: Neutron star, Magnetar, Spin polarization, Equation of state, Nuclear matter, Tidal deformability, Love number, Gravitational wave.

Tóm tắt

Phương trình trạng thái của vật chất sao neutron có phân cực spin trong từ trường mạnh đã được nghiên cứu bằng phương pháp trường trung bình trong mẫu Hartree-Fock bằng 4 tương tác hiệu dụng phụ thuộc mật độ CDM3Y4, 5, 6 và 8. Hai kịch bản đơn giản của độ phân cực spin Δ phụ thuộc vào mật độ baryon đã được xem xét; đồng thời, kết quả của chúng được so sánh với các ràng buộc từ các nghiên cứu về cấu trúc hạt nhân và quan sát sóng hấp dẫn trong thiên văn (sự kiện GW170817 và GW190425). Các kịch bản tương ứng với phân cực một phần ($\Delta < 1.0$) cũng tỏ ra hợp lí, với các kết quả của năng lượng đối xứng và độ nén của chất hạt nhân đối xứng ứng với các tương tác hầu hết đều nằm trong các khoảng giá trị thực nghiệm. Phương trình trạng thái của vật chất hạt nhân phi đối đứng dựa trên phương pháp trường trung bình đã được áp dụng để xây dựng vật chất cân bằng βcủa sao neutron, cấu thành bởi tương tác mạnh giữa các baryon (proton và neutron), electron và muon.

Phương trình trạng thái vật chất sao neutron sau đó được sử dụng làm đầu vào cho các tính toán về các tính chất vĩ mô của sao neutron như khối lượng M, bán kính R, thông số Love loại gravito-electric k_l và gravito-magnetic j_l ứng với các tương tác hạt nhân kể trên cũng được tính bằng lý thuyết Tương đối rộng. Từ các ràng buộc thực nghiệm từ sự kiện GW170817 và giới hạn khối lượng của 2 pulsar nặng nhất từng được ghi nhận, ta đưa ra kết luận rằng chỉ các tương tác CDM3Y6 và CDM3Y8 là phù hợp nhất trong nghiên cứu về sao neutron. Các thông số Love gắn liền với biến dạng thủy triều của sao neutron trong các hệ sao đôi quay quanh nhau cũng được tính lên tới các đóng góp ở bậc 4 và mối liên hệ giữa giá trị của chúng với khối lượng sao cũng được chỉ ra.

Từ khóa: Sao neutron, Magnetar, Phân cực spin, Phương trình trạng thái, Vật chất hạt nhân, Biến dạng thủy triều, Thông số Love, Sóng hấp dẫn.

Chapter 1

Introduction

Neutron stars (NS) are the compact astronomical objects known also as pulsars, formed shortly after the core-collapse supernova as a super dense, giant liquid drop of strongly interacting baryons and leptons. With the NS gravitational mass M up to twice the solar mass $M_\odot$, NS matter is enclosed tightly within a radius of $R \sim 10 - 12$ km and the baryon density n_b inside the NS core is several times larger than the normal matter density in center of a heavy nucleus like ^{208}Pb ($n_0 \approx 0.17$ fm^{-3}). Neutron stars are in fact the densest accessible astronomical objects in the Universe after black holes (Baym and Pethick, 1975), and the physics effects by all the four fundamental interactions have been found from the astrophysical observations of the single- and binary pulsars. Therefore, NS is an ideal natural "laboratory" for the modern physics research that links different fields of physics, like atomic and nuclear physics, high-energy physics, and astrophysics (Lattimer and Prakash, 2004).

The massive neutrino emission during the cooling of hot proto-neutron star (PNS) formed instantly after supernova proceeds mainly via the weak process of electron capture by protons in the PNS core

$$p + e^- \rightarrow n + \nu_e, \tag{1.1}$$

leading to a huge excess of neutrons in the core, and hence the name "neutron star". In fact, neutrons in the dense core of NS are not bound by the strong force between baryons but they are packed tightly by a hydrostatic balance between the pressure of NS matter and gravitation. In this study, we focus on cold NS after a considerable time from its formation, when the temperature is considered to be $T = 0$.

Below the atmospheric gas layer of NS, the low-density matter of NS *crust* is highly inhomogeneous. With the increasing density, the NS matter gradually becomes more or less uniform so that the dense core of NS can be treated as an uniform, neutron-rich nuclear matter (NM) which is referred to hereafter as asymmetric NM (see illustration in Figure 1.1). It is obvious that one needs to use a proper nuclear physics model to determine the pressure of fully degenerated baryons and that of leptons in NS matter at different matter densities in order to determine the macroscopic properties of NS within the frame of General Relativity (GR). Over the years, different nuclear mean-field models have been used to construct the *equation of states* (EoS) of asymmetric NM, which gives the behavior of macroscopic properties of NM like the pressure P and mass-energy density

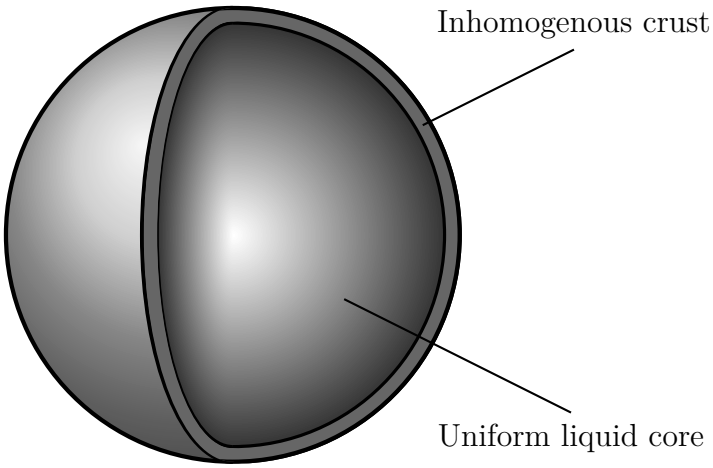

Figure 1.1: Simplified illustration of NS structure, where the baryon density decreases (from white to dark gray) as we move outward from the center of NS.

ε with the increasing NM density. Among these studies, the nonrelativistic Hartree-Fock (HF) approach to study NM using an appropriate effective (in-medium) nucleon-nucleon (NN) interaction has been well proven to give a realistic description of asymmetric NM up to very high baryon densities (Khoa et al., 1996). Because the NN interaction in a dense medium of NM is very different from the free NN interaction, the use of an effective density dependent NN interaction is widely adopted in the mean-field calculations of NM, although some ab-initio many-body calculations of NM using the QCD-based interaction between baryons are now feasible with the supercomputer of very high performance. In the present work, we perform the HF calculation of asymmetric NM using the well-tested CDM3Yn model of the effective density dependent NN interaction (Tan et al., 2021), which is presented in details in Chapter 2. A rapidly rotating NS or pulsar is known to have a strong intrinsic magnetic field, and significant fractions of protons and neutrons in NS matter might have their spins polarized along the axis of magnetic field **?**. To explore the effects by the spin polarization of baryons, we have extended the conventional HF method to the calculation of the EoS of spin-polarized NM. which is further used to generate NS matter that consists of strongly interacting baryons (protons and neutrons) and leptons (electrons and muons) being in β-equilibrium. The EoS of the inhomogeneous crust of NS taken from the compressible liquid drop model (Douchin et al., 2000; Douchin and Haensel, 2001) is added to the EoS of the β-stable NS matter given by the present HF calculation, to obtain the full input for NS matter. Such a mean-field input of the EoS of NS matter can then be used in GR to determine the gravitational mass and radius of NS (Tan et al., 2020, 2021) from the solution of the Tolman-Oppenheimer-Volkoff (TOV) equations (**?**).

Given a realistic EoS of NS matter, the General Relativity not only explains the com-

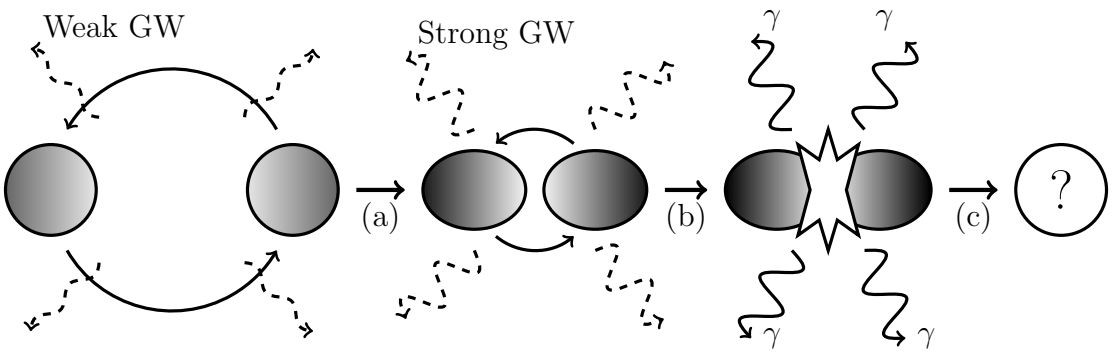

Figure 1.2: Illustration of the merger of a binary NS system. (a) The two companion NS orbit about each others, while gradually losing energy by emitting weak GW and coming slowly closer with time. (b) As the two NS get closer, they accelerate and emit stronger GW until (c) merging with each other, which results in an extremely energetic explosion known as *kilonova*, an event associated with blue jets of *gamma ray burst* (GRB) of very high intensity. The end product of the merger is either a small black hole (BH) or a heavier NS.

pact shape of NS in the hydrostatic equilibrium, but also predicts the interesting behavior of NS in a strong gravitational field. In particular, the shape of NS is tidally deformed to gain a nonzero quadrupole moment under the gravitational field formed by the mutual attraction of two coalescing NS's Damour and Nagar (2009). The first astronomical observation of a binary NS merger has been reported on August 17, 2017, with the gravitational wave (GW) signals detected by LIGO and Virgo laser interferometers Abbott et al. (2017), and the γ ray burst (GRB) of very high intensity detected by the Fermi γ ray space telescope **?**. This exciting event is now widely referred to as GW170817, which opened a new era of the multimessenger astronomy. Following the GW signals from GW170817 (Abbott et al., 2017), such signals have been detected two years later from a compact merger of two NS's dubbed as GW190425 (Abbott et al., 2020). The Bayesian analyses of these GW data resulted on the empirical constraints for the tidal deformation of NS, as well as the gravitational mass M and radius R of NS (Abbott et al., 2018). The NS merger event is illustrated in Figure 1.2, and one can see that gravitation exerted by each NS tends to tidally "stretch" its companion while both orbiting spirally toward each other and dissipating energy through the emited GW. As a result, the shape and mass-energy distribution of NS are tidally deformed from its supposedly spherical shape, leading to the nonzero multipole moments (Hinderer, 2008; Hinderer et al., 2010; Damour and Nagar, 2009). The tidal deformability of NS, i.e., how strongly it deforms upon the impact of tidal field, is usually expressed in terms of the *tidal Love numbers* k_l of several orders l. In the present study, we evaluate the Love number of NS up to the 4^{th} order, $l = 2, 3, 4$ (Perot and Chamel, 2021). It is naturally to expect that the tidal Love number depends on the EoS of NS matter, and this effect is discussed in Chapter 3. Given very high baryon density in the center of NS (up to $6n_0$ where n_0 is the saturation density of normal NM) the Love number of NS is of order ~ 0.1, while our Earth has that of ~ 0.3. In a recent study, the Love number has been predicted to be ~ 0.002 for

spinning black holes with nearly infinite matter density inside (Le Tiec and Casals, 2021).

It is amazing that, like a charged sphere being electrically and magnetically deformed under a strong electromagnetic field, the tidal deformability of NS under the perturbation of spacetime can also be separated into the *gravito-electric* (GE) and *gravito-magnetic* (GM) components (Damour and Nagar, 2009). Namely, the tidal deformability (the Love number) of NS in the presence of tidal field can be characterized by the corresponding GE (k_l) and GM (j_l) components (Perot and Chamel, 2021). This interesting result is presented in Chapter 3. In summary, the study performed in this Thesis is focused on:

- Inclusion of the spin polarization of baryons into the HF calculation of EoS of asymmetric NM (Tan et al., 2021),
- Dependence of the gravitational mass and radius of NS on different assumptions for the EoS of NS matter,
- Sensitivity of GE and GM Love numbers of the tidal deformability to the EoS of NS matter,
- Comparison of the calculated macroscopic properties of NS with the empirical astrophysical constraints inferred from the observed GW signals of the NS merger (Abbott et al., 2018; Xie and Li, 2019).

Chapter 2

Mean-field study of nuclear matter

2.1 Hartree-Fock calculation of asymmetric nuclear matter

In this section, we only limit ourselves to two-body interaction, thus, the nucleon-nucleon (NN) potential can be expressed in the form of

$$v = v(\boldsymbol{r}, \boldsymbol{r'}, \boldsymbol{p}, \boldsymbol{p'}, \boldsymbol{\sigma}, \boldsymbol{\sigma'}, \boldsymbol{\tau}, \boldsymbol{\tau'}) \tag{2.1}$$

where the primed and unprimed variables indicate the properties of 2 nucleons respectively, in which $\boldsymbol{r}$ is the particle's position, $\boldsymbol{p}$ is its momentum, $\boldsymbol{\sigma}$ is its intrinsic spin and $\boldsymbol{\tau}$ is its isospin.

The functional form of v in (2.1) cannot freely take any form but is constrained by many invariance requirements (Greiner and Maruhn, 1996), namely the translational, Galilei, rotational, isospin, parity and time reversal invariance. Having such considerations, the central component of NN interaction potential is expressed as function of the distance r between interacting nucleons

$$v = v_{00}(r) + v_{10}(r)\boldsymbol{\sigma} \cdot \boldsymbol{\sigma'} + v_{01}(r)\boldsymbol{\tau} \cdot \boldsymbol{\tau'} + v_{11}(r)(\boldsymbol{\sigma} \cdot \boldsymbol{\sigma'})(\boldsymbol{\tau} \cdot \boldsymbol{\tau'}) \tag{2.2}$$

There exists another composition of the interaction, i.e. the *spin-orbit* terms, however, as stated by **?**, their contributions are much smaller than the central one, and have yet to be included in the present study. Due to the lack of an exact theory to describe the NN interaction, a model needs to be imposed and fit with experimental measurement or theoretical calculation results. Furthermore, for a system as massive as a NS, deducing the EoS of the matter using the *ab initio* method, i.e. solving the Schrödinger equation over all particles, is impossible; therefore an *effective interaction* must be used (Greiner and Maruhn, 1996). Here, among various interaction models, the CDM3Yn interaction was chosen. This interaction is constructed based on the M3Y-Paris interaction, which was used successfully in the HF study of NM (Loan et al., 2011; Tan et al., 2016, 2020, 2021) and the folding model study of NN scattering (Khoa et al., 1997; Khoa and Satchler, 2000), with the direct (exchange) central terms being expressed as

$$v^{D(EX)} = v_{00}^{D(EX)}(r) + v_{10}^{D(EX)}(r)\boldsymbol{\sigma} \cdot \boldsymbol{\sigma'} + v_{01}^{D(EX)}(r)\boldsymbol{\tau} \cdot \boldsymbol{\tau'} + v_{11}^{D(EX)}(r)(\boldsymbol{\sigma} \cdot \boldsymbol{\sigma'})(\boldsymbol{\tau} \cdot \boldsymbol{\tau'}) \tag{2.3}$$

The density-dependence of the NN interaction is encoded into an additional form factor $F_{\sigma\tau}(n_b)$ multplied to each $\sigma\tau$-term, which gives rise to the explicit form of the CDM3Yn interactions, i.e.

$$\begin{aligned} v^{D(EX)}(n_b, r) = F_{00}(n_b)v_{00}^{D(EX)}(r) + F_{10}(n_b)v_{10}^{D(EX)}(r)\boldsymbol{\sigma}\cdot\boldsymbol{\sigma'} \\ + F_{01}(n_b)v_{01}^{D(EX)}(r)\boldsymbol{\tau}\cdot\boldsymbol{\tau'} + F_{11}(n_b)v_{11}^{D(EX)}(r)(\boldsymbol{\sigma}\cdot\boldsymbol{\sigma'})(\boldsymbol{\tau}\cdot\boldsymbol{\tau'}) \end{aligned} \quad (2.4)$$

where each radial term is the superposition of 3 Yukawa potentials

$$v_{\sigma\tau}^{D(EX)}(r) = \sum_{k=1}^{3} Y_{\sigma\tau}^{D(EX)}(k)\frac{\exp(-\mu_k r)}{\mu_k r} \quad (2.5)$$

with the Yukawa strengths given in Table 2.1. The form factors $F_{\sigma\tau}(n_b)$ shared the functional form (Khoa et al., 1997; Tan et al., 2020, 2021; Thân, 2010)

$$F_{\sigma\tau}(n) = C_{\sigma\tau}[1 + \alpha_{\sigma\tau}\exp(-\beta_{\sigma\tau}n) + \gamma_{\sigma\tau}n] \quad (2.6)$$

with parameters given in Table 2.2. The parameters of F_{00} were adjusted to give the corresponding values of incompressibility K of symmetric NM at saturation density n_0 and the binding energy $E_0 \approx 15.8\ MeV$, while the 10 term is modified from (Thân, 2010) to reproduce $E_{sym}(n_0) \approx 30\ MeV$, $L \approx 50\ MeV$ and to be in agreement with the ab-initio results (Akmal et al., 1998; Gandolfi et al., 2010) at higher density (Tan et al., 2021).

Table 2.1: Yukawa strengths of the M3Y-Paris interaction (Tan et al., 2020; Anantaraman et al., 1983).

k	μ_k (fm^{-1})	Y_{00}^{D} (MeV)	Y_{10}^{D} (MeV)	Y_{01}^{D} (MeV)	Y_{11}^{D} (MeV)
1	4.0	11061.625	938.875	313.625	−969.125
2	2.5	−2537.5	−36.0	223.5	450.0
3	0.7072	0.0	0.0	0.0	3.4877
k	μ_k (fm^{-1})	Y_{00}^{EX} (MeV)	Y_{10}^{EX} (MeV)	Y_{01}^{EX} (MeV)	Y_{11}^{EX} (MeV)
1	4.0	−1524.25	−3492.75	−4118.0	−2210.0
2	2.5	−518.75	795.25	1054.75	568.75
3	0.7072	−7.8474	2.6157	2.6157	−0.8719

On the other hand, in Table 2.2, the spin-dependent terms (10 and 11) are hereby included in 4 models by fine tuning the parameters to yield close result to the Brueckner-Hartree-Fock (BHF) study of spin polarized NM by Vidana and Bombaci (2002) as in Figure 2.1.

In HF formalism, the total HF energy of the system can be expressed as

$$\begin{aligned} E_{HF} = \sum_{\sigma\tau}\sum_{\boldsymbol{k}}^{k_F^{\sigma\tau}}\frac{\hbar^2k^2}{2m_\tau} + \frac{1}{2}\sum_{\boldsymbol{k}\sigma\tau}\sum_{\boldsymbol{k'}\sigma'\tau'}\Big[\Big\langle\boldsymbol{k}\sigma\tau,\boldsymbol{k'}\sigma'\tau'\Big|v^D\Big|\boldsymbol{k}\sigma\tau,\boldsymbol{k'}\sigma'\tau'\Big\rangle \\ + \Big\langle\boldsymbol{k}\sigma\tau,\boldsymbol{k'}\sigma'\tau'\Big|v^{EX}\Big|\boldsymbol{k'}\sigma\tau,\boldsymbol{k}\sigma'\tau'\Big\rangle\Big] \end{aligned} \quad (2.7)$$

Table 2.2: CDM3Yn interaction's parameters; the 00 and 01 terms are inherited from (Tan et al., 2021), while the 10 and 11 parameters are added by fitting with BHF result and K is the incompressibility (2.17) of spin-saturated symmetric NM at saturation density $n_0 \approx 0.17\ fm^{-3}$.

Interaction	$\sigma\tau$	$C_{\sigma\tau}$	$\alpha_{\sigma\tau}$	$\beta_{\sigma\tau}$ (fm^3)	$\gamma_{\sigma\tau}$ (fm^3)	K (MeV)
CDM3Y4	00	0.3052	3.2998	2.3180	-2.0	228
	01	0.2129	6.3581	7.0584	5.6091	
	10	0.2593	6.0016	-2.3377	18.8725	
	11	0.8329	3.5941	9.2012	0.2690	
CDM3Y5	00	0.2728	3.7367	1.8294	-3.0	241
	01	0.2204	6.6146	7.9910	6.0040	
	10	0.4106	5.6265	-1.6698	-1.9866	
	11	0.6815	2.5833	5.1700	0.2578	
CDM3Y6	00	0.2658	3.8033	1.4099	-4.0	252
	01	0.2313	6.6865	8.6775	6.0182	
	10	0.5186	9.9402	1.6698	2.9799	
	11	0.6058	3.1947	4.4512	0.0822	
CDM3Y8	00	0.2658	3.8033	1.4099	-4.3	257
	01	0.2643	6.3836	9.8950	5.4249	
	10	0.5997	9.1900	0.7514	-4.7181	
	11	0.3786	3.9435	2.7012	0.3512	

with Ω being the spatial volume of the system, $k_F^{\sigma\tau} = (6\pi^2 n_{\sigma\tau})^{1/3}$ is the Fermi momentum corresponding to spin σ and isospin τ, the first double summation is the *kinetic energy* of the system, while the other being its *potential energy*.

Dividing (2.7) by the system total volume Ω, the energy density of the NM is separated into the kinetic term ε_{kin} and the potential terms $\varepsilon_{\sigma\tau}$, i.e.

$$\varepsilon_{HF} = \frac{E_{HF}}{\Omega} = \varepsilon_{kin} + F_{00}(n_b)\varepsilon_{00} + F_{01}(n_b)\varepsilon_{01} + F_{10}(n_b)\varepsilon_{10} + F_{11}(n_b)\varepsilon_{11} \tag{2.8}$$

The final expressions of each terms of the energy density are

$$\varepsilon_{kin} = \frac{3}{10}\sum_{\sigma\tau}\frac{\hbar^2(k_F^{\sigma\tau})^2}{m_\tau}n_{\sigma\tau} \tag{2.9}$$

$$\varepsilon_{00} = \frac{1}{2}\left[n_b^2 J_{00}^D + \int A_{00}^2 v_{00}^{EX}(r)\, d^3r\right] \tag{2.10}$$

$$\varepsilon_{10} = \frac{1}{2}\left[n_b^2 J_{10}^D \left(\Delta_n \frac{1+\delta}{2} + \Delta_p \frac{1-\delta}{2}\right)^2 + \int A_{10}^2 v_{10}^{EX}(r)\, d^3r\right] \tag{2.11}$$

$$\varepsilon_{01} = \frac{1}{2}\left[n_b^2 J_{01}^D \delta^2 + \int A_{01}^2 v_{01}^{EX}(r)\, d^3r\right] \tag{2.12}$$

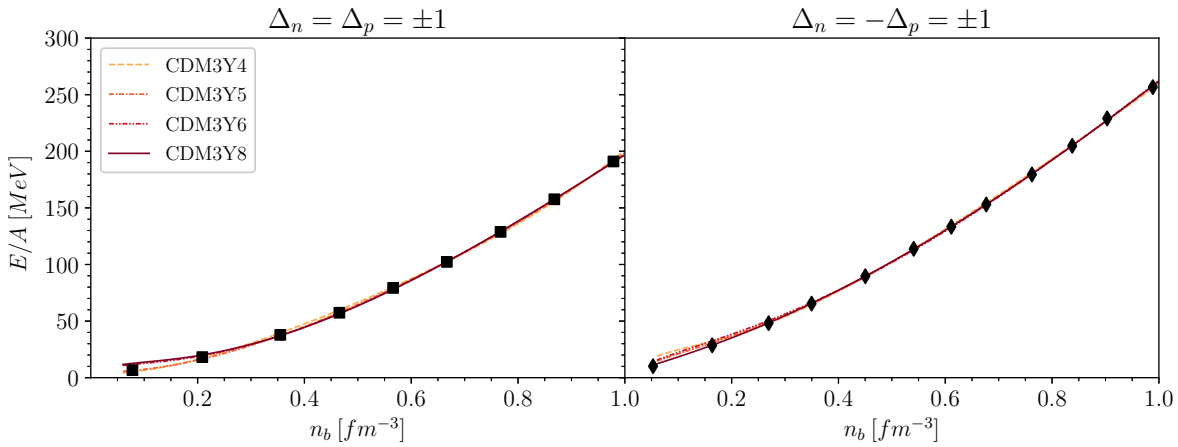

Figure 2.1: Energy per baryon E/A of symmetric NM by the 4 CDM3Yn models compared to BHF result (Vidana and Bombaci, 2002). The diamond and square represent the BHF result for $\Delta_n = -\Delta_p = \pm 1$ and $\Delta_n = \Delta_p = \pm 1$ respectively with Δ_τ being the baryon spin polarization.

$$\varepsilon_{11} = \frac{1}{2}\left[n_b^2 J_{11}^D \left(\Delta_n \frac{1+\delta}{2} - \Delta_p \frac{1-\delta}{2}\right)^2 + \int A_{11}^2 v_{11}^{EX}(r)\, d^3r\right] \tag{2.13}$$

where $\Delta_\tau = (n_{\uparrow\tau} - n_{\downarrow\tau})/n_\tau$ is the polarization of nucleon, $\delta = (n_n - n_p)/n_b$ is the asymmetry of NM, $J_{\sigma\tau}^D = \int v_{\sigma\tau}^D(r)\, d^3r$ is the volume integral of the direct interaction and

$$\begin{aligned}
A_{00} &= n_{\uparrow n}\hat{j}_1(k_F^{\uparrow n} r) + n_{\downarrow n}\hat{j}_1(k_F^{\downarrow n} r) + n_{\uparrow p}\hat{j}_1(k_F^{\uparrow p} r) + n_{\downarrow p}\hat{j}_1(k_F^{\downarrow p} r) \\
A_{10} &= n_{\uparrow n}\hat{j}_1(k_F^{\uparrow n} r) - n_{\downarrow n}\hat{j}_1(k_F^{\downarrow n} r) + n_{\uparrow p}\hat{j}_1(k_F^{\uparrow p} r) - n_{\downarrow p}\hat{j}_1(k_F^{\downarrow p} r) \\
A_{01} &= n_{\uparrow n}\hat{j}_1(k_F^{\uparrow n} r) + n_{\downarrow n}\hat{j}_1(k_F^{\downarrow n} r) - n_{\uparrow p}\hat{j}_1(k_F^{\uparrow p} r) - n_{\downarrow p}\hat{j}_1(k_F^{\downarrow p} r) \\
A_{11} &= n_{\uparrow n}\hat{j}_1(k_F^{\uparrow n} r) - n_{\downarrow n}\hat{j}_1(k_F^{\downarrow n} r) - n_{\uparrow p}\hat{j}_1(k_F^{\uparrow p} r) + n_{\downarrow p}\hat{j}_1(k_F^{\downarrow p} r)
\end{aligned} \tag{2.14}$$

with $\hat{j}_1(x) = 3j_1(x)/x$ and $j_1(x)$ being the 1$^{\text{st}}$ order spherical Bessel function.

In the parabolic approximation (Khoa et al., 1996), the energy density per nucleon E/A can also be expanded in terms of the asymmetry δ as

$$\frac{E}{A}(n_b, \delta, \Delta_n, \Delta_p) = \frac{\varepsilon_{HF}}{n_b} = \frac{E}{A}(n_b, \delta = 0, \Delta_n, \Delta_p) + S(n_b, \Delta_n, \Delta_p)\delta^2 + \mathcal{O}(\delta^4) \tag{2.15}$$

with S being the *nuclear symmetry energy*. The nuclear symmetry energy is well constrained at low baryon density by the study of heavy-ion (HI) collisions (Tsang et al., 2011; Ono et al., 2003), the structure study of the giant dipole resonance by Trippa et al. (2008) or the neutron skin (Furnstahl, 2002). As shown in Figure 2.2, the symmetry energy S (2.15) of symmetric ($\delta = 0$) NM is calculated for each interaction in different polarizations and compared to the empirical data, along with other nuclear models (APR and MMC). It's clear that the more strongly NM polarizes under magnetic field, the higher

the symmetry energy S is. Moreover, at high values of Δ, S falls completely outside of the HI range suggested, while the cases of weaker or without polarization appear to remain well within this range, as well as the 90% CFL region of the astrophysical constraint of GW170817 (Xie and Li, 2019).

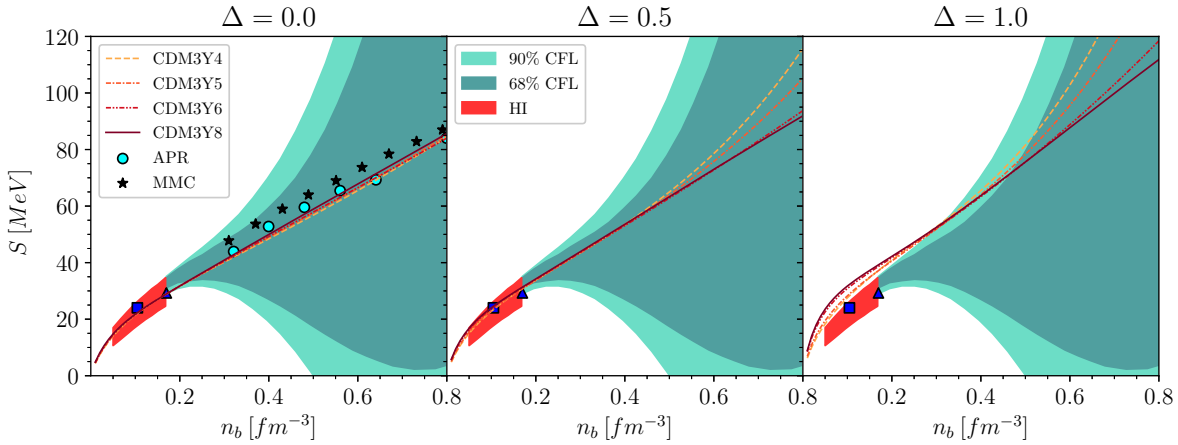

Figure 2.2: Symmetric energy S of symmetric NM at increasing polarization with 4 CDM3Yn interaction models. The shaded areas are the empirical ranges obtained from the Bayesian study (Xie and Li, 2019) of the NS of radius $R_{1.4}$ at 68% and 90% confident level (CFL) with the GW170817 event (Abbott et al., 2018). The square and triangle are the values suggested by the structure study of Trippa et al. (2008) and Furnstahl (2002). The circles and stars are the ab-initio result of Akmal et al. (1998) (APR) and microscopic Monte Carlo (MMC) calculation by Gandolfi et al. (2010).

The same conclusion can be drawn from the energy per baryon E/A of symmetric NM (Figure 2.3), as it is in good agreement with the APR (Akmal et al., 1998) and MMC results (Gandolfi et al., 2010) at the spin saturated ($\Delta \approx 0$) scenario, similar to the work of Tan et al. (2021) on an older version of CDM3Y8 interaction. The astrophysical constraint from GW170817, on the other hand, is much narrower than that for the nuclear symmetry energy S and thus well constraints the value of E/A at high baryon density. As Δ increases from 0.0 to 1.0, the energy per baryon rises significantly, which indicates a scenario of spin saturated NM for $n_b > n_0$.

On the other hand, the density-dependence of S is also investigated through the symmetry coefficient J, slope parameter L and curvature K_{sym}, which are taken by expanding the symmetry energy at saturation density n_0, i.e. (Tan et al., 2020; Li et al., 2008; Horowitz et al., 2014; Lattimer, 2014)

$$S(n_b, \Delta_n, \Delta_p) = J(\Delta_n, \Delta_p) + \frac{L(\Delta_n, \Delta_p)}{3}\left(\frac{n_b - n_0}{n_0}\right) + \frac{K_{sym}(\Delta_n, \Delta_p)}{18}\left(\frac{n_b - n_0}{n_0}\right)^2 + \dots \tag{2.16}$$

as well as the nuclear incompressibility defined at saturation density

$$K(\Delta_n, \Delta_p) = 9\left.\frac{\partial P_b(n_b, \delta = 0, \Delta_n, \Delta_p)}{\partial n_b}\right|_{n_b \to n_0} \tag{2.17}$$

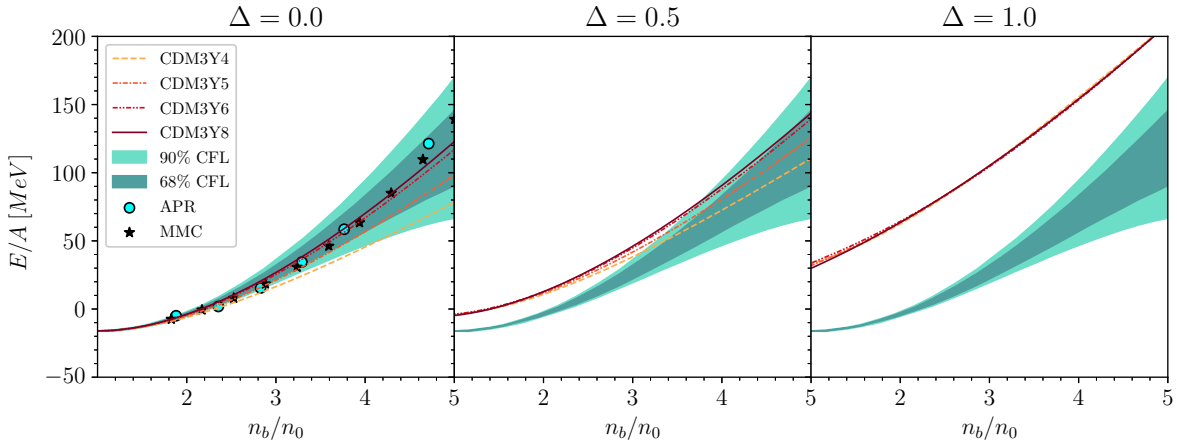

Figure 2.3: Same as Figure 2.2 for the energy per baryon E/A of symmetric NM.

with P_b being the baryonic pressure.

Among these quantities, the incompressibility K of symmetric NM has been intensively studied the most in several structure studies of monopole excitations (e.g. Garg and Colo (2018)), HI collisions and refractive NN scattering (Khoa et al., 2007). The HF result in Table 2.3 leaves only the case of $\Delta = 0.0$ to satisfy the constrained value $K \approx 240^{+20}_{-20} MeV$ deduced from these studies, since in this case, K ranges from $227 - 257\ MeV$, which is well within the empirical value. Apart from the nuclear incompressibility K, recently, the values of J, L, K_{sym} are much more well determined from the study of Essick et al. (2021) by combining astrophysical data with PREX-II and chiral effective field theory, which yields $J \approx 34^{+3}_{-3} MeV$, $L \approx 58^{+19}_{-19} MeV$ and $K_{sym} \approx -107^{+128}_{-138} MeV$. The value of J and L obtained with HF formalism (Table 2.3) remain well within the interval suggested by this study, except for when the polarization Δ approaches ≈ 1.0. The curvature K_{sym}, however, has not been as well determined as the other quantities, therefore it still widely ranges for different scenarios and no further selection on the EoS with it can be done.

2.2 β-stable spin-polarized neutron star matter

After the HF calculation, we were able to obtain a numerical HF energy density ε_{HF}. However, it is in fact impossible for a NS to exist while consisting of purely nucleon. In order to compensate for this issue, leptons (e^- and μ^-) have to be introduced to the matter constituents and the $npe\mu$ matter has to satisfy the *β-stable* condition (Glendenning, 2012), i.e.

- Charge balance

$$n_p = n_e + n_\mu \tag{2.18}$$

- Chemical potential balance

$$\mu_n - \mu_p = \mu_e = \mu_\mu \tag{2.19}$$

Table 2.3: The symmetry coefficient J, slope parameter L, curvature K_{sym} of the symmetric energy (2.16) and incompressibility K (2.17) of symmetric NM, calculated using 4 different NN interactions.

Interaction	Δ	J	L	K_{sym}	K
CDM3Y4	0.0	28.97	48.38	−60.49	227.96
	0.5	30.83	52.63	−54.54	294.58
	1.0	37.26	63.81	−66.58	498.50
CDM3Y5	0.0	28.92	48.36	−49.61	241.25
	0.5	30.78	51.42	−43.60	316.30
	1.0	37.20	59.37	−47.54	545.96
CDM3Y6	0.0	28.94	48.36	−42.09	251.86
	0.5	31.19	49.93	−33.86	319.51
	1.0	38.67	52.27	−25.26	526.68
CDM3Y8	0.0	28.95	48.39	−28.65	257.13
	0.5	31.35	49.58	−21.86	343.25
	1.0	39.23	50.53	−16.40	602.65

where $\mu_i = \frac{\partial \varepsilon}{\partial n_i}$ $(i = n, p, e, \mu)$ is the chemical potential of the i particle.

The total energy density of the $npe\mu$ matter is thus

$$\varepsilon = \varepsilon_{HF} + n_n m_n c^2 + n_p m_p c^2 + \varepsilon_e + \varepsilon_\mu \tag{2.20}$$

which leads to the nucleon chemical potential of the form

$$\mu_\tau(n_n, n_p, \Delta_n, \Delta_p) = \frac{\partial \varepsilon}{\partial n_\tau} = \frac{\partial \varepsilon_{HF}}{\partial n_\tau} + m_\tau c^2 \tag{2.21}$$

Let $\hat{\mu} = \mu_n - \mu_p$ be the leptons' chemical potential, (2.18) is equivalent to[1]

$$3\pi^2(\hbar c)^3 n_p - \hat{\mu}^3 - \left[\hat{\mu}^2 - (m_\mu c^2)^2\right]^{3/2} \theta(\hat{\mu} - m_\mu c^2) = 0 \tag{2.22}$$

Note that only beyond the muon threshold density $\mu_e > m_\mu c^2 \approx 105.6\, MeV$ do muons appear in the system. Furthermore, under strong magnetic field like that of a magnetar, we can approximate $\Delta_n \approx -\Delta_p \approx \Delta$ and reduce the EoS to depend on just the baryon polarization Δ alone, and the more baryon polarized, the stronger the magnetic field of the NS.

For a fixed value of Δ, we are able to obtain a density function of the form $n_n(n_b, \Delta)$ and $n_p(n_b, \Delta)$, which in turn gives the lepton chemical potential $\hat{\mu}(n_b, \Delta) = \hat{\mu}(n_n, n_p)$ On the other hand, the leptons' densities are then

$$n_e(n_b, \Delta) = \frac{\hat{\mu}^3(n_b, \Delta)}{3\pi^2(\hbar c)^3} \quad \text{and} \quad n_\mu(n_b, \Delta) = \frac{\left[\hat{\mu}^2(n_b, \Delta) - (m_\mu c^2)^2\right]^{3/2}}{3\pi^2(\hbar c)^3} \theta(\hat{\mu}(n_b, \Delta) - m_\mu c^2) \tag{2.23}$$

[1] $\theta(x)$ is the Heaviside function, i.e. it returns 1 for $x \geq 0$ and 0 otherwise.

Consider the e^- and μ^- to be systems of relativistic Fermi gas, then their respective energy densities and pressure contributions are ($l = e, \mu$) (Moustakidis and Panos, 2009)

$$\varepsilon_l(n_b, \Delta) = \frac{2}{(2\pi)^3} \int_0^{[3\pi^2 n_l(n_b,\Delta)]^{1/3}} \sqrt{\hbar^2 c^2 k^2 + m_l^2 c^4}\, d^3\mathbf{k} \tag{2.24}$$

and

$$P_l(n_b, \Delta) = \frac{1}{3}\frac{2}{(2\pi)^3} \int_0^{[3\pi^2 n_l(n_b,\Delta)]^{1/3}} \frac{\hbar^2 c^2 k^2}{\sqrt{\hbar^2 c^2 k^2 + m_l^2 c^4}}\, d^3\mathbf{k} \tag{2.25}$$

Plus, from the HF study, the baryonic pressure is given by

$$P_b = n_b^2 \frac{\partial}{\partial n_b}\left[\frac{E}{A}(n_b, \delta, \Delta)\right] \tag{2.26}$$

Finally, we obtain the total energy density-dependence on baryon density as

$$\varepsilon(n_b, \Delta) = \varepsilon_{HF}(n_b, \Delta) + n_n(n_b, \Delta) m_n c^2 + n_p(n_b, \Delta) m_p c^2 + \varepsilon_e(n_b, \Delta) + \varepsilon_\mu(n_b, \Delta) \tag{2.27}$$

and the total pressure of NS matter

$$P(n_b, \Delta) = P_b(n_b, \Delta) + P_e(n_b, \Delta) + P_\mu(n_b, \Delta) \tag{2.28}$$

The mass-energy density of NS matter is also defined as $\rho = \varepsilon/c^2$, which will be used as input for the TOV equation in Chapter 3.

In addition, the EoS of the NS's crust (very low baryon density region with $n_b \lesssim 0.01\, fm^{-3}$) is adopted from the Compress Liquid Drop Model calculation (Douchin et al., 2000; Douchin and Haensel, 2001), which was also shown by Tan et al. (2020) that the magnetization of the crust has little effects on NS properties. In Figure 2.4, we show the total pressure of NS matter $P(n_b)$ following the HF calculation of 4 different versions of the density-dependent NN interaction endowed with different levels of polarization. These results are simultaneously compared with the empirical pressure obtained from the "spectral" EoS inferred from the Bayesian analysis of the GW170817 event (Abbott et al., 2018). It is clear that the larger K an interaction version has (Table 2.3), the more the generated NM can be compressed to higher pressure at high density, and the model CDM3Y4 can be excluded since it is unlikely to satisfy the constraint derived by Abbott et al. (2018), while the other versions still lie inside of the 90% CFL region at $\Delta \approx 0.0$. In general, the pressures calculated by these 4 models follow well the empirical values from $\approx \rho_0$ to their corresponding maximum central density, i.e. the total pressure at twice and six times nuclear saturation density is within the range $P(2\rho_0) \approx 3.5^{+2.7}_{-1.7} \times 10^{34}$ and $P(6\rho_0) \approx 9.0^{+7.9}_{-2.6} \times 10^{35}\ dyn/cm^2$ at 90% CFL. Plus, at increasing spin polarization, the pressure tends to be stronger, indicated by a raise of $P(\rho_b)$ most significantly at the low density region. Taking all of the EoS constraint up until now into account, the value suggested by the empirical study tends to favor models with higher K value and smaller spin polarization.

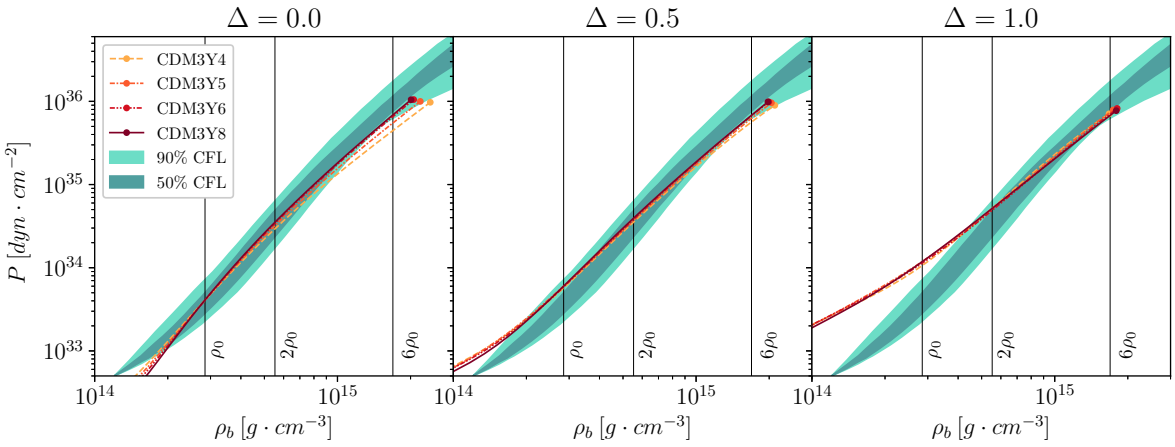

Figure 2.4: Same as Figure 2.2 for the pressure P as a function of *rest baryon mass density* ρ_b along with empirical pressure given by the "Spectral" EoS from the Bayesian analysis of the GW170817 data (Abbott et al., 2018) with 50% (light gray) and 90% (dark gray) confidence level. The dot at the end of each line corresponds to the central baryon density n_b of maximum NS mass.

Chapter 3

Neutron star as relativistic compact object and its tidal deformability

The observation of the NS merger GW170817 has provided for the first time the empirical estimate of the tidal deformation of NS induced by strong gravitational field between the two companions of a merging binary pulsar (Hinderer, 2008; Hinderer et al., 2010). In this chapter, we discuss briefly, within the frame of General Relativity, how a static spherical NS can be tidally deformed by gravitation, gaining nonzero gravito-multipole moments which are directly proportional to the strength of gravitation (Damour and Nagar, 2009). The tidal deformation moments of different multipoles are determined in the present work with the mean-field based EoS of spin-polarized NS matter using the explicit expressions of the Love numbers given by GR (Perot and Chamel, 2021). The obtained results for the tidal deformability as well as the gravitational mass M and radius R of NS are compared in details with the astrophysical constraints deduced from the observation of GW170817.

3.1 Einstein equations of relativistic neutron star

In general, the line element of metric in the static isotropic spacetime can be expressed within GR (Glendenning, 2012) in terms of spatial spherical coordinates as

$$ds^2 = g_{\mu\nu}dx^\mu dx^\nu = e^{2\nu(r)}c^2dt^2 - e^{2\lambda(r)}dr^2 - r^2d\theta^2 - r^2\sin^2\theta d\phi^2, \tag{3.1}$$

where arbitrary functions $\nu(r)$ and $\lambda(r)$ are determined locally by the mass-energy density enclosed within the sphere of radius r. In the vicinity of a static spherical NS, the spacetime geometry is determined from the pressure and mass-energy density of NS matter (treated as a perfect fluid), and the energy-momentum tensor is obtained in GR as

$$T^{\mu\nu} = -Pg^{\mu\nu} + (P+\rho)u^\mu u^\nu,\ g_{\mu\nu}u^\mu u^\nu = u_\nu u_\nu = 1. \tag{3.2}$$

Here P and ρ are the pressure and mass-energy density of NS matter, respectively, $u^\mu = dx^\mu/d\tau$ is the local fluid 4-velocity. The Einstein's field equations of neutron star are written as

$$G^{\mu\nu} = -\frac{8\pi G}{c^4}T^{\mu\nu}. \tag{3.3}$$

Keeping the nonrelativistic limit to the static Newtonian gravitation, the Einstein's field equations (3.3) can be reduced to the following differential equations which are known as Tolman-Oppenheimer-Volkoff (TOV) equations (Glendenning, 2012)

$$\begin{aligned} \frac{dP(r)}{dr} &= -\frac{G\rho(r)\mathcal{M}(r)}{c^2r^2}\left[1+\frac{P(r)}{\rho(r)}\right]\left[1+\frac{4\pi P(r)r^3}{c^2\mathcal{M}(r)}\right]\left[1-\frac{2G\mathcal{M}(r)}{c^2r}\right]^{-1}, \\ d\mathcal{M}(r) &= 4\pi r^2\rho(r)dr, \end{aligned} \tag{3.4}$$

where r is the radial coordinate in Schwarzschild metric (3.1), and $\mathcal{M}(r)$ is the gravitational mass enclosed within sphere of radius r. $\rho(r)$ and $P(r)$ are the mass-energy density and pressure of NS matter at distance r from the star center, respectively. TOV equations (3.4) are integrated from $r = 0$ to the surface of NS, with the star radius R given by $P(R) = 0$. Other boundary conditions are

$$\mathcal{M}(0) = 0, \quad \rho(0) = \rho_c, \quad P(0) = P_c, \quad \mathcal{M}(R) = M. \tag{3.5}$$

From the solutions of the TOV equations (3.4) based on the pressure and mass-energy density of NS matter given by the considered EoS, the correlated profiles of the mass and pressure of NS can be obtained as functions of distance r from the star center. The total mass M and radius R of NS are then deduced from the boundary conditions for the TOV solutions.

Partial spin polarization of baryons in NS matter

The HF results in Chap. 2 have been obtained with the uniform (density independent) spin polarization of baryons of different strengths Δ. However, the magnetic field distribution inside a magnetar is much more complex (Fujisawa and Kisaka, 2014), and the use of a density independent Δ cannot be justified. In fact, baryons in the inner core of the magnetar are tightly compressed by gravity at high densities of NS matter which leads to the full degeneracy so that there is no possibility for baryon to flip its spin orientation. Therefore, along with the intrinsic magnetic field, the spin polarization of baryons is expected to gradually weaken to $\Delta \approx 0$ at high densities in the center of NS (Fujisawa and Kisaka, 2014; Tan et al., 2020). Although it's beyond the scope of the current study to precisely calculate the density dependence of $\Delta(n_b)$, we explore this effect by investigating two different scenarios proposed recently by Tan et al. (2020), based on the magnetic field distribution of magnetar modelled by Fujisawa and Kisaka (2014)

(A) The magnetic field is strongly localized in the surface region of the magnetar, near the crust-core transition, and $\Delta \to 0$ at $n_b \approx 0.18$ fm^{-3},

(B) The magnetic field distribution is broader, covering both the crust and outer core of NS, and Δ decreases gradually to zero at a larger density $n_b \approx 0.35$ fm^{-3}.

Each scenario is assumed to have a starting value of the spin polarization of baryons at low densities, $\Delta_0 = 0.6$, 0.8 and 1 as shown in Figure 3.1. The EoS's of β-stable

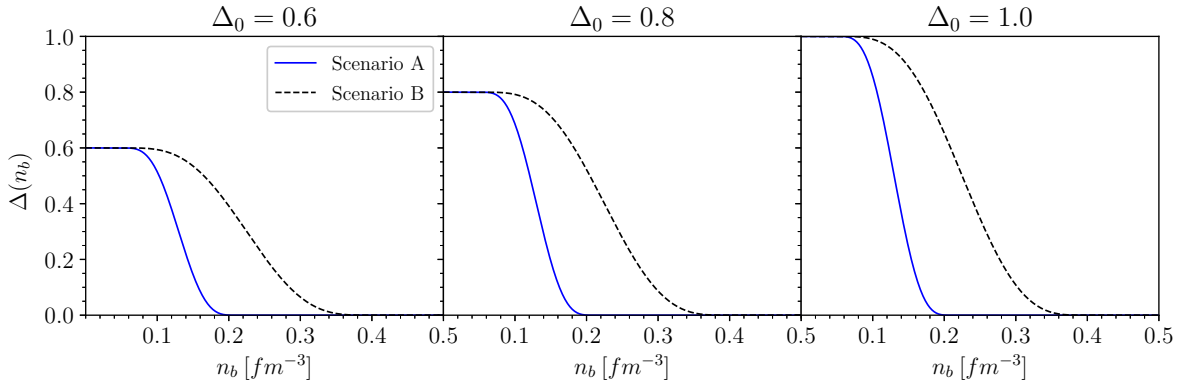

Figure 3.1: Different scenarios of the density dependence of the spin polarization of baryons.

$npe\mu$ matter obtained with different spin polarizations of baryons have been used as input for the TOV equations (3.4), and the results obtained for the mass and radius of magnetar are shown in Figure 3.2. For comparison, we have plotted in this Figure also the empirical constraint for the mass and radius of NS around $M \approx 1.4M_\odot$ implied by the tidal deformability of NS estimated from the GW signals of GW170817 (Abbott et al., 2018) (see more details on the tidal deformation of NS in Sect. 3.2), and the empirical mass limit of the second PSR J0348+0432 ($M \approx 2.01^{+0.04}_{-0.04}M_\odot$) and millisecond PSR J0740+6620 ($M \approx 2.14^{+0.20}_{-0.18}M_\odot$), the heaviest NSs observed so far. While the $M - R$ results given by 4 versions of the EoS with partial spin polarizations of baryons ($\Delta_0 = 0.6 \sim 0.8$) are within the empirical GW170817 constraint for NS with $M = 1.4M_\odot$, the NS configurations starting with $\Delta_0 = 1.0$ seem to be out of the empirical range, as concluded recently by Tan et al. (2020) and Tews and Schwenk (2020). The radius of NS with a $M \approx 1.4M_\odot$ obtained in scenario A with partial spin polarization of $\Delta_0 = 0.6$ is $R_{1/4} \approx 11.2 - 12.7$ km, which agrees well with the empirical value $R_{1.4} \approx 11.75^{+0.86}_{-0.81}$ km deduced from the joint analysis of two NS mergers GW170817 and GW190425 (Dietrich et al., 2020). The spin polarization of baryons significantly enlarges the radius but affects minorly the mass of NS as noted by Tan et al. (2020). In addition, the observed masses of two heaviest pulsars PSR J0348+0432 and PSR J0740+6620 allow us to trace the impact of the nuclear incompressibility K on the NS mass. Among four versions of the in-medium NN interaction used in the present HF calculation of NM, only the CDM3Y6 and CDM3Y8 interactions (associated with $K \approx 252$ and 257 MeV) give the maximum gravitational mass of NS close to the lower mass limit of the two heavy pulsars. These K values are slightly higher than that around 240 MeV inferred from the structure studies of giant monopole resonances of finite nuclei **?**. In this connection we note a recent model-independent systematics of the astrophysical observations and results of the ab-initio calculations by Annala et al. **?**, which shows that the NS matter in the interior of massive NS with $M \approx 2M_\odot$ seems to contain deconfined baryons which form a quark-matter core in the center of NS. Such a quark core can stiffen the EoS at highest densities of NS matter and contributes up to 0.25 $M_\odot$ to the total NS mass **?**. Therefore, a slight increase

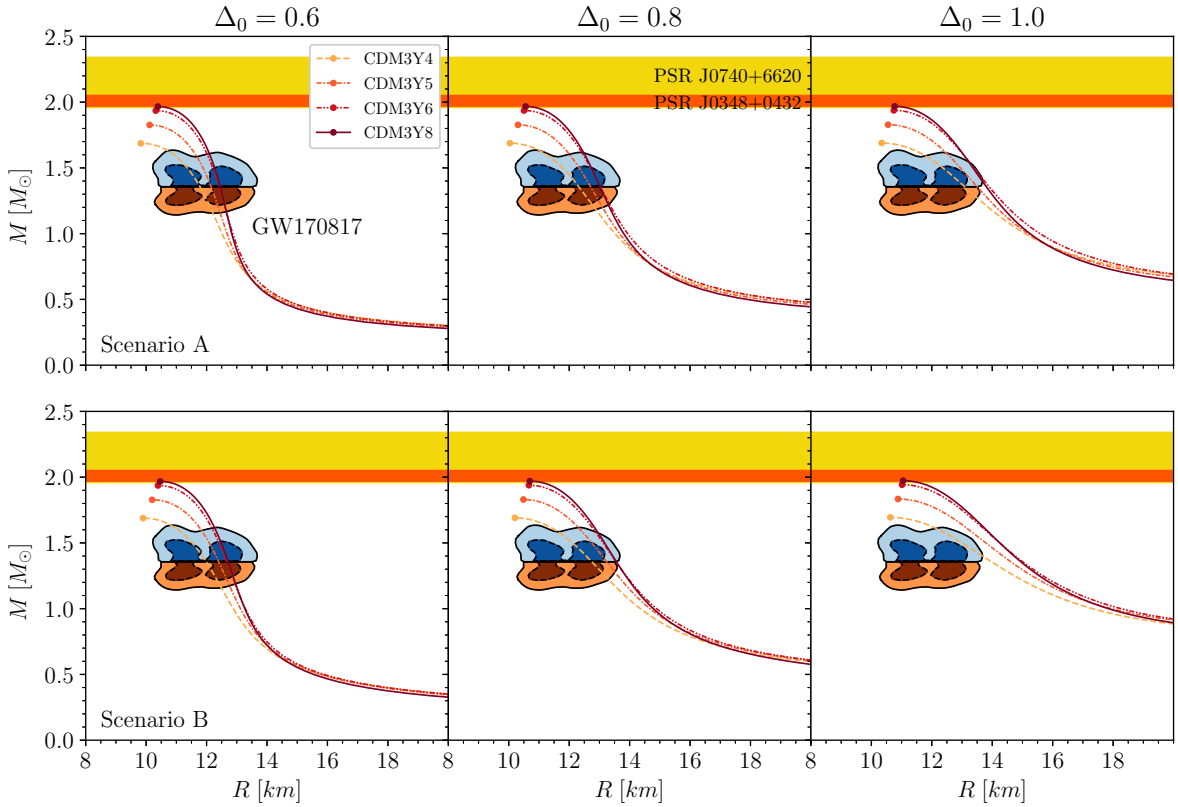

Figure 3.2: The correlation of the gravitational mass M and radius R of magnetar given by the solutions of the TOV equations (3.4) obtained with different EoS's of spin-polarized NS matter. The empirical constraints for NS with mass of $1.4M_\odot$ inferred from the GW170817 data are shown by the colored contour, where the blue (red) shaded area represents the heavier (lighter) NS (Abbott et al., 2018). The dot in each line indicates the maximum NS mass given by the corresponding EoS. The dark and light orange regions are the observed mass of the second PSR J0348+0432 (Antoniadis et al., 2013) and millisecond PSR J0740+6620 (Cromartie et al., 2020) respectively.

of the K value given by the CDM3Y6 and CDM3Y8 interactions from the adopted value might be explained by a possible existence of the quark core in the center of heavy NS.

3.2 Gravito-electric and gravito-magnetic deformability

In this chapter we address an interesting analogy between gravitation and electromagnetism which has a long story because of similarity between Newton law for gravitational force and Coulomb law for electrostatic force **?**. Here we discuss briefly the basic elements of gravitoelectromagnetism (GEM) as presented by Damour and Nagar (2009). Assuming the linear perturbation of spacetime by gravitation, the global inertial frame $x^\mu = (ct, \mathbf{x})$

and Minkowski metric $\eta_{\mu\nu}$ can be expressed as

$$g_{\mu\nu} \approx \eta_{\mu\nu} + h_{\mu\nu}(x), \tag{3.6}$$

and the Einstein's field equations (3.3) reads

$$\Box \bar{h}_{\mu\nu} = -\frac{16\pi G}{c^4} T_{\mu\nu} \tag{3.7}$$

where $\bar{h}_{\mu\nu} = h_{\mu\nu} - \frac{1}{2}\eta_{\mu\nu}\eta^{\rho\sigma}h_{\rho\sigma}$. Remarkably, the representation (3.7) of the Einstein's field equation is completely analogous to the well-known Maxwell's equations of classical electromagnetism

$$\Box A^{\nu} = 4\pi j^{\nu} \tag{3.8}$$

with A being the electromagnetic field strength tensor and j being the current 4-vector. By introducing the GEM potentials Φ and $\mathbf{A}$ via $\bar{h}_{00} = 4\Phi/c^2$ and $\bar{h}_{0i} = -2A_i/c^2$, we define the GEM fields as

$$E_i = 4\partial_i\Phi + \frac{2}{c}\frac{\partial A_i}{\partial t}, \quad B_i = -2c\epsilon_{ijk}\partial_j A_k. \tag{3.9}$$

In the nonrelativistic limit to Newtonian gravitation, the GE potential is reduced to the classical gravitational potential $\sim GM/r$. In an analogy to the classical theory of electromagnetism, the gravitational field surounding NS can be decomposed into the *gravito-electric* (GE) and *gravito-magnetic* (GM) components (Damour and Nagar, 2009)

$$\mathcal{E}_L = \partial_{L-1}E_{a_l} \qquad \text{and} \qquad \mathcal{B}_L = \partial_{L-1}B_{a_l} \tag{3.10}$$

where E_{a_l} and B_{a_l} are the a_l component of the local GE and GM fields, L represents the multi-index $(a_1, a_2, \ldots, a_l)$ and l being the order of the moment. In a binary system of two merging NS, each companion of the pair feels the tidal force of the gravitation field acting between them and becomes tidally deformed. It is natural from Eq. (3.10) that such tidal deformation of NS is directly proportional to the strength of the gravitational field, and can be characterized by the GE and GM *tidal deformabilities* λ_l and σ_l of the l-th order (Damour and Nagar, 2009)

$$\mathcal{Q}_L = \lambda_l \mathcal{E}_L, \tag{3.11}$$

$$\mathcal{S}_L = \sigma_l \mathcal{B}_L \tag{3.12}$$

with $\mathcal{Q}_L$ being the induced mass multipole moment, i.e. the deviation of the mass distribution from the spherical shape at order l, while $\mathcal{S}_L$ is the current multipole moment in adiabatic approximation (Damour and Nagar, 2009; Perot and Chamel, 2021).

The equations (3.11) and (3.12) give a direct link between the tidal field strengths and the multipole moments of the object, in which the reaction of the body is directly propertional to the field strengths. Plus, it is evident that the higher λ_l (or σ_l) is, the stronger the NS deforms under the same tidal field. From these deformabilities, the dimensionless GE and GM *tidal Love numbers* are defined as (Perot and Chamel, 2021)

$$k_l = \frac{1}{2}(2l-1)!!\frac{G\lambda_l}{R^{2l+1}} \quad \text{and} \quad j_l = 4(2l-1)!!\frac{G\sigma_l}{R^{2l+1}} \tag{3.13}$$

These parameters are directly related to the GE and GM *tidal deformability parameters* as

$$\Lambda_l = \frac{2}{(2l-1)!!} k_l \left(\frac{c^2 R}{GM}\right)^{2l+1} \tag{3.14}$$

$$\Sigma_l = \frac{1}{4(2l-1)!!} j_l \left(\frac{c^2 R}{GM}\right)^{2l+1} \tag{3.15}$$

which can be extracted from the signal of GW. In order to properly calculate these parameters, let $H_l(r)$ and $\tilde{H}_l(r)$ characterize small perturbations of the static metric. These functions have to satisfy (Perot and Chamel, 2021; Damour and Nagar, 2009)

$$\begin{aligned} &H_l''(r) + H_l'(r)\left[1-\frac{2Gm(r)}{c^2 r}\right]^{-1}\left\{\frac{2}{r} - \frac{2Gm(r)}{c^2 r^2} - \frac{4\pi G}{c^4} r[\varepsilon(r) - P(r)]\right\} \\ &\quad + H_l(r)\left[1-\frac{2Gm(r)}{c^2 r}\right]^{-1}\left\{\frac{4\pi G}{c^4}\left[5\varepsilon(r) + 9P(r) + c^2\frac{\mathrm{d}\varepsilon}{\mathrm{d}P}[\varepsilon(r)+P(r)]\right]\right. \\ &\quad \left. - \frac{l(l+1)}{r^2} - 4\left[1-\frac{2Gm(r)}{c^2 r}\right]^{-1}\left[\frac{Gm(r)}{c^2 r^2} + \frac{4\pi G}{c^4} r P(r)\right]^2\right\} = 0 \end{aligned} \tag{3.16}$$

for GE perturbations and

$$\begin{aligned} &\tilde{H}_l''(r) - \tilde{H}_l'(r)\left[1-\frac{2Gm(r)}{c^2 r}\right]^{-1}\frac{4\pi G}{c^4} r\,[P(r)+\varepsilon(r)] \\ &\quad - \tilde{H}_l(r)\left[1-\frac{2Gm(r)}{c^2 r}\right]^{-1}\left\{\frac{l(l+1)}{r^2} - \frac{4Gm(r)}{c^2 r^3} + \theta\frac{8\pi G}{c^4}[P(r)+\varepsilon(r)]\right\} = 0 \end{aligned} \tag{3.17}$$

for GM perturbations; the value of $\theta = 1$ is for static fluid while irrotational fluid adopts the value $\theta = -1$. These equations govern the even and odd parity parts of the stationary perturbation of the background metric, as developed by Damour and Nagar (2009), and are integrated along with the TOV equation (3.4). In addition, we have the compactness parameters $C = GM/(Rc^2)$ and define

$$y_l = \frac{RH_l'(R)}{H_l(R)} \quad \text{and} \quad \tilde{y}_l = \frac{R\tilde{H}_l'(R)}{\tilde{H}_l(R)}. \tag{3.18}$$

The explicit expressions of the first few orders of the GE and GM Love numbers are

$$\begin{aligned} k_2 = {}& \frac{8}{5}C^5(1-2C)^2[2(y_2-1)C - y_2 + 2]\left\{2C\left[4(y_2+1)C^4 + 2(3y_2-2)C^3\right.\right. \\ & \left. -2(11y_2-13)C^2 + 3(5y_2-8)C - 3(y_2-2)\right] \\ & \left. +3(1-2C)^2[2(y_2-1)C - y_2 + 2]\log(1-2C)\right\}^{-1}, \end{aligned} \tag{3.19}$$

$$k_3 = \frac{8}{7}C^7(1-2C)^2\left[2(y_3-1)C^2 - 3(y_3-2)C + y_3 - 3\right] \times \left\{2C\left[4(y_3+1)C^5\right.\right.$$

$$\times +2(9y_3-2)C^4-20(7y_3-9)C^3+5(37y_3-72)C^2-45(2y_3-5)C+15(y_3-3)\Big]$$
$$+15(1-2C)^2\left[2(y_3-1)C^2-3(y_3-2)C+y_3-3\right]\log(1-2C)\Big\}^{-1}, \tag{3.20}$$

$$k_4=\frac{32}{147}C^9(1-2C)^2\left[12(y_4-1)C^3-34(y_4-2)C^2+28(y_4-3)C-7(y_4-4)\right]$$
$$\times\Big\{2C\left[8(y_4+1)C^6+4(17y_4-2)C^5-12(83y_4-107)C^4+40(55y_4-116)C^3\right.$$
$$\left.-10(191y_4-536)C^2+105(7y_4-24)C-105(y_4-4)\right]+15(1-2C)^2\left[12(y_4-1)C^3\right.$$
$$\left.-34(y_4-2)C^2+28(y_4-3)C-7(y_4-4)\right]\log(1-2C)\Big\}^{-1}, \tag{3.21}$$

$$j_2=\frac{24}{5}C^5\left[2(\tilde{y}_2-2)C-\tilde{y}_2+3\right]\Big\{2C\left[2(\tilde{y}_2+1)C^3+2\tilde{y}_2C^2+3(\tilde{y}_2-1)C-3(\tilde{y}_2-3)\right]$$
$$+3\left[2(\tilde{y}_2-2)C-\tilde{y}_2+3\right]\log(1-2C)\Big\}^{-1}, \tag{3.22}$$

$$j_3=\frac{64}{21}C^7\left[8(\tilde{y}_3-2)C^2-10(\tilde{y}_3-3)C+3(\tilde{y}_3-4)\right]$$
$$\times\Big\{2C\left[4(\tilde{y}_3+1)C^4+10\tilde{y}_3C^3+30(\tilde{y}_3-1)C^2-15(7\tilde{y}_3-18)C+45(\tilde{y}_3-4)\right]$$
$$+15\left[8(\tilde{y}_3-2)C^2-10(\tilde{y}_3-3)C+3(\tilde{y}_3-4)\right]\log(1-2C)\Big\}^{-1}, \tag{3.23}$$

$$j_4=\frac{80}{147}C^9\left[40(\tilde{y}_4-2)C^3-90(\tilde{y}_4-3)C^2+63(\tilde{y}_4-4)C-14(\tilde{y}_4-5)\right]$$
$$\times\Big\{2C\Big[4(\tilde{y}_4+1)C^5+18\tilde{y}_4C^4+90(\tilde{y}_4-1)C^3-5(137\tilde{y}_4-334)C^2$$
$$+105(7\tilde{y}_4-26)C-210(\tilde{y}_4-5)\Big]+15\Big[40(\tilde{y}_4-2)C^3-90(\tilde{y}_4-3)C^2$$
$$+63(\tilde{y}_4-4)C-14(\tilde{y}_4-5)\Big]\log(1-2C)\Big\}^{-1} \tag{3.24}$$

as derived by Perot and Chamel (2021).

The results for GE tidal Love number's dependence on NS's gravitational mass arose from 4 versions of the EoS are shown in Figure 3.3. Similar to Perot and Chamel (2021), in this result, it is clear that the higher the order l, the less impactful the Love number k_l is for the tidal properties of the NS, i.e. k_l tends to be smaller by an order of magnitude than k_{l-1}, as expected from the multipole expansion. The 2$^{\text{nd}}$ order is consequently dominant compared to the others. Between two scenarios A and B, at partial polarization of $\Delta_0 = 0.6$, the difference in k_l of the same order is insignificant, except for the small difference in the low mass section. On the other hand, for the case of higher spin polarity in the NS surface, the results are much more distinguishable, as the computation with scenario B gives rise to a "steeper" curve of k_l. Furthermore, in general, the maximum values of k_l are at the common gravitational mass M at all orders computed so far, and this value of M seems to only depends on the value of Δ_0, where the position of maximum k_l tends to be shifted to a higher M as Δ_0 increases. Among these tidal parameters, the only one that has been constrained by far is the dominant 2$^{\text{nd}}$ order Love number, which is investigated through the closely related dimensionless tidal deformability parameter of second order Λ_2 (3.14) and whose results are given in Figure 3.4. In the study of Abbott et al. (2018), the range of Λ_2 is accepted to be $\Lambda_2 \approx 190^{+390}_{-120}$ at $M = 1.4M_\odot$. It is interesting to note that for all cases in this study, this constraint tolerates all EoSs and

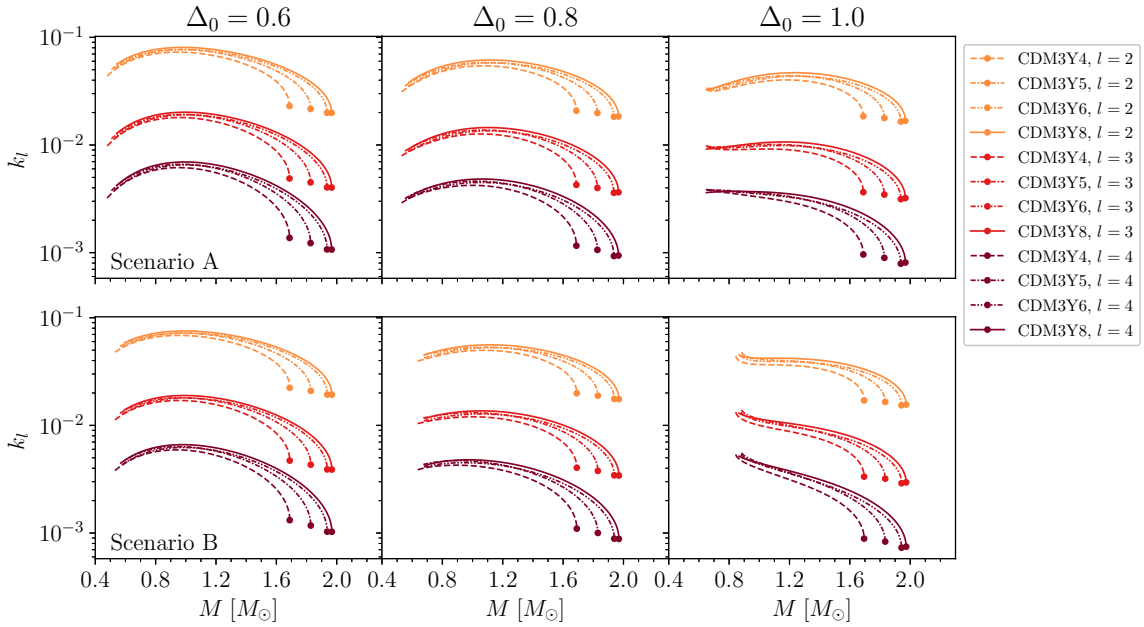

Figure 3.3: GE tidal Love number at l^{th} order k_l as function of magnetar mass computed with 4 density-dependent NN interaction versions at different spin polarizations. The dot at the end of each line represents the maximum gravitational mass M of the magnetar generated by the corresponding EoS.

scenarios, as well as the value of Δ_0, thus no further exclusion can be done with this parameter. It's worth mentioning that the nuclear incompressibility K plays a significant role in determining the tidal deformability Λ_2 as when K varies from version to version (CDM3Y4 to CDM3Y8), the value of Λ_2 increases by ≈ 3 times for the scenario A of $\Delta_0 = 0.6$ case, the same can be said for the different configuration of $\Delta(n_b)$. Testing the values of k_l at higher orders can also be done by evaluating the tidal correction of the GW waveform from inspiralling NSs within the PN theory, i.e. the GE contribution of order $(2l+1)$PN to the phase of GW signal is (Perot and Chamel, 2021; Yagi, 2014)

$$\Psi_l = -\sum_{i=1}^{2}\left[\frac{5}{16}\frac{(2l-1)!!(4l+3)(l+1)}{(4l-3)(2l-3)}\Lambda_{l,i}X_i^{2l-1}x^{2l-3/2} + \frac{9}{16}\delta_{l2}\Lambda_{2,i}\frac{X_i^4}{\eta}x^{5/2}\right] + \mathcal{O}(x^{2l-1/2}) \tag{3.25}$$

where $i = 1, 2$ is the index distinguishing the two NSs of the system, $x = (G\pi M f/c^3)^{2/3}$, f is the GW signal frequency, $M = M_1 + M_2$, $X_i = M_i/M$ and $\eta = M_1M_2/M^2$.

The gravito-magnetic tidal Love numbers j_l contribute more weakly to the GW phase compared to that of their GE counterpart, as the GM terms only appear from higher orders of $(2l+2)$PN, where the first correction at 6PN is given by (Perot and Chamel, 2021; Yagi, 2017)

$$\tilde{\Psi}_2 = \sum_{i=1}^{2}\frac{5}{224}\sigma_{2,i}\frac{X_i^4}{\eta}\left(X_i - 1037X_j\right)x^{7/2} + \mathcal{O}(x^{9/2}) \tag{3.26}$$

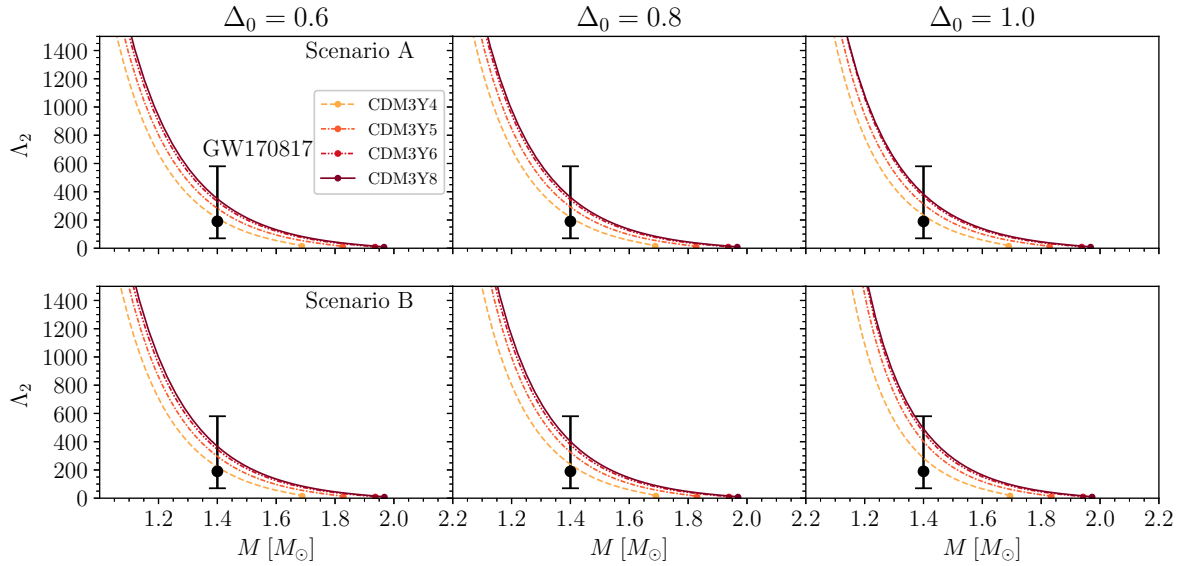

Figure 3.4: Dimensionless GE tidal deformability parameter of 2nd order Λ_2 of different CDM3Yn models with varying Δ. The vertical bar is the empirical tidal deformability constraint $\Lambda_2 \approx 190^{+390}_{-120}$ at $1.4M_\odot$, obtained from the Bayesian analysis of GW170817 data with 90% confidence level (Abbott et al., 2018).

The GM tidal Love numbers of second, third and fourth order computed with 4 different

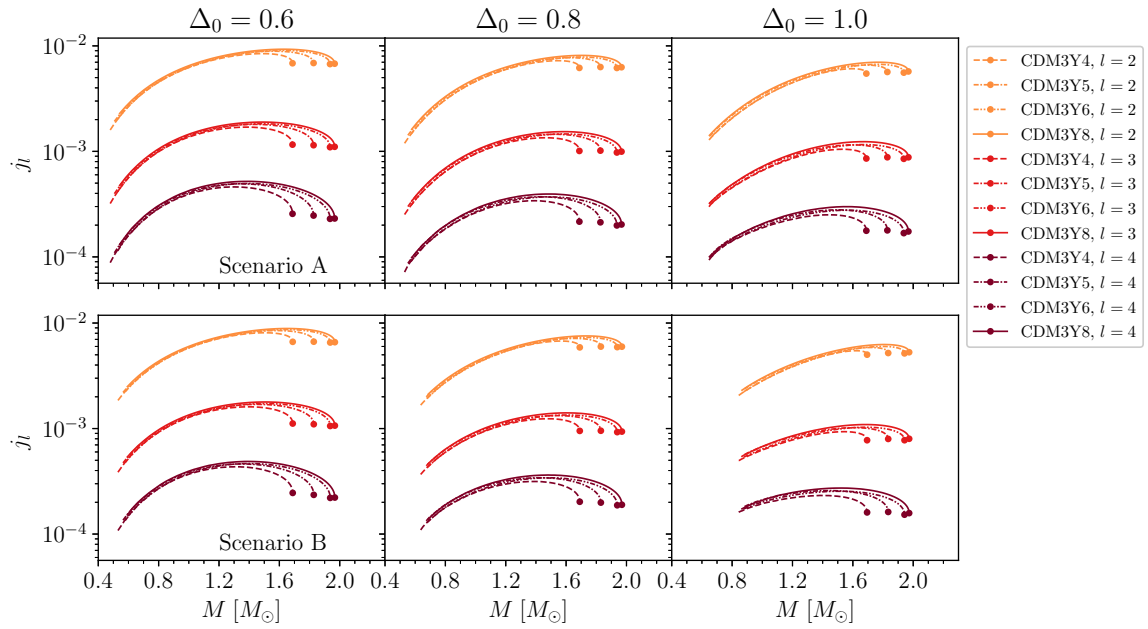

Figure 3.5: GM tidal Love number at l^{nd} order j_l as function of NS mass computed with CDM3Yn models of *strictly static fluid* at different polarizations.

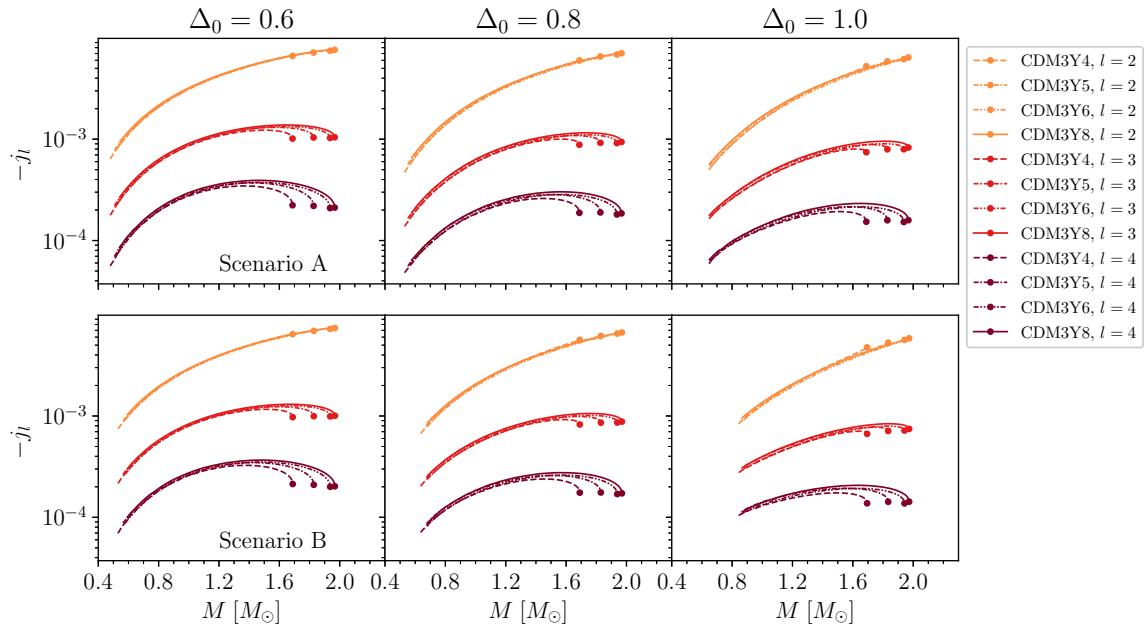

Figure 3.6: GM tidal Love number at l^{nd} order j_l as function of NS mass computed with CDM3Yn models of *irrotational fluid* at different polarizations.

EoSs are shown in Figure 3.5 for strictly static fluid and 3.6 for irrotational fluid. Apart from the same trends as the GE tidal Love numbers discussed previously, the GM Love numbers' values do not have much variation as Δ_0 increases in each scenario, as the shape of each curves in Figure 3.5 doesn't differ far from each others except for the difference in range of gravitational mass M. The value of j_l corresponding to the GM pertubation of irrotational fluid (Figure 3.6), on the other hand, stands out from the other two types of Love numbers, where its value is completely negative, albeit having the same magnitude as that of static fluid, this type of fluid motion is stated to be more realistic in this case due to it being driven by the tides (Perot and Chamel, 2021; Pani et al., 2018). In this case, the lines traced by each interation appear to reach maximum value at the maximum M at the leading terms only, rather than having a local maxima in between. The dominance of the 2^{nd} order terms are clear in all cases, where the difference of around one order of magnitude is maintained. Notably, for the GM terms corresponding with each NN interaction, at higher order l, the NS mass at maximum j_l seems to become smaller. One more interesting result is that the magnitudes of j_l for two types of fluid are also comparable but is smaller than their GE counterpart by one order of magnitude, similar to the conclusion reached by Perot and Chamel (2021).

Chapter 4

Conclusions

By extending the 4 current versions of density-dependent NN interaction (Tan et al., 2021), we have been able to include the description of spin polarization effect of NS matter under strong magnetic field over a wider range of K into the EoS of NM using the nonrelativistic HF formalism. In general, concerning the EoS of NM, the empirical ranges deduced for symmetry energy S, energy per baryon of symmetric NM E/A and total pressure P seem to favor partial to zero polarization, or in particular, the cases with lower Δ overall. Among these 4 versions of EoS, the CDM3Y4 interaction is very unlikely to occur in reality, as the EoS generated by these interactions are usually outside of the 90% CFL boundary obtained from astrophysical observation and analysis at high density.

The density-dependence of the polarization Δ is also taken into account by using different situations regarding the localization of magnetic field at the surface of magnetar (Tan et al., 2020), which eventually eliminates the possibility of total polarization at the magnetar's surface, i.e. $\Delta_0 \approx 1.0$. The macroscopic properties of the NS, on the other hand, only the cases of partial polarization at the scenario A succeed in staying within the GW170817 constraint (Abbott et al., 2018), which supports the suggestion of the blue kilonova ejecta of GW170817 coming from a magnetar (Metzger et al., 2018; Tan et al., 2020). Furthermore, only the CDM3Y6 and CDM3Y8 in these scenarios can come close to satisfy the lower mass limit of the two heaviest pulsars ever observed, i.e. PSR J0348+0432 and PSR J0740+6620. The tidal deformability parameter Λ_2, surprisingly, do not provide further constraint, as all cases are within the accepted range obtained by Abbott et al. (2018). Beside, higher orders of multipoles up to the 4^{th} order have been investigated for both gravito-electric and gravito-magnetic tidal perturbations. The common diminishing effects as the order l increases are founded for all cases, as well as the dominance of the GE tidal Love numbers in magnitude compared to the GM ones, which is understandable with the contribution of each term in the phase of GW signal (Abdelsalhin et al., 2018). The observation of GM tidal deformability can be possibly used as an additional test for Einstein's theory of GR, since these effects are not presented in Newtonian physics. More information on the EoS of NS matter can also be further constrained with the potential observation of the higher order terms, which might be possible with the 3^{rd}-generation GW detectors.

Bibliography

Abbott, B., Abbott, R., Abbott, T., Abraham, S., Acernese, F., Ackley, K., Adams, C., Adhikari, R., Adya, V., Affeldt, C., et al. (2020). GW190425: observation of a compact binary coalescence with total mass $\sim 3.4 M_{\odot}$. *The Astrophysical Journal Letters*, 892(1):L3.

Abbott, B. P., Abbott, R., Abbott, T., Acernese, F., Ackley, K., Adams, C., Adams, T., Addesso, P., Adhikari, R., Adya, V., et al. (2017). GW170817: observation of gravitational waves from a binary neutron star inspiral. *Physical Review Letters*, 119(16):161101.

Abbott, B. P., Abbott, R., Abbott, T., Acernese, F., Ackley, K., Adams, C., Adams, T., Addesso, P., Adhikari, R. X., Adya, V. B., et al. (2018). GW170817: Measurements of neutron star radii and equation of state. *Physical review letters*, 121(16):161101.

Abdelsalhin, T., Gualtieri, L., and Pani, P. (2018). Post-Newtonian spin-tidal couplings for compact binaries. *Physical Review D*, 98(10):104046.

Akmal, A., Pandharipande, V., and Ravenhall, D. a. (1998). Equation of state of nucleon matter and neutron star structure. *Physical Review C*, 58(3):1804.

Anantaraman, N., Toki, H., and Bertsch, G. (1983). An effective interaction for inelastic scattering derived from the Paris potential. *Nuclear Physics A*, 398(2):269–278.

Antoniadis, J., Freire, P. C., Wex, N., Tauris, T. M., Lynch, R. S., van Kerkwijk, M. H., Kramer, M., Bassa, C., Dhillon, V. S., Driebe, T., et al. (2013). A massive pulsar in a compact relativistic binary. *Science*, 340(6131).

Baym, G. and Pethick, C. (1975). Neutron stars. *Annual Review of Nuclear Science*, 25(1):27–77.

Cromartie, H. T., Fonseca, E., Ransom, S. M., Demorest, P. B., Arzoumanian, Z., Blumer, H., Brook, P. R., DeCesar, M. E., Dolch, T., Ellis, J. A., et al. (2020). Relativistic Shapiro delay measurements of an extremely massive millisecond pulsar. *Nature Astronomy*, 4(1):72–76.

Damour, T. and Nagar, A. (2009). Relativistic tidal properties of neutron stars. *Physical Review D*, 80(8):084035.

Dietrich, T., Coughlin, M. W., Pang, P. T., Bulla, M., Heinzel, J., Issa, L., Tews, I., and Antier, S. (2020). Multimessenger constraints on the neutron-star equation of state and the Hubble constant. *Science*, 370(6523):1450–1453.

Douchin, F. and Haensel, P. (2001). A unified equation of state of dense matter and neutron star structure. *Astronomy & Astrophysics*, 380(1):151–167.

Douchin, F., Haensel, P., and Meyer, J. (2000). Nuclear surface and curvature properties for SLy Skyrme forces and nuclei in the inner neutron-star crust. *Nuclear Physics A*, 665(3-4):419–446.

Essick, R., Tews, I., Landry, P., and Schwenk, A. (2021). Astrophysical Constraints on the Symmetry Energy and the Neutron Skin of ^{208}Pb with Minimal Modeling Assumptions. *arXiv preprint arXiv:2102.10074*.

Fujisawa, K. and Kisaka, S. (2014). Magnetic field configurations of a magnetar throughout its interior and exterior–core, crust and magnetosphere. *Monthly Notices of the Royal Astronomical Society*, 445(3):2777–2793.

Furnstahl, R. (2002). Neutron radii in mean-field models. *Nuclear Physics A*, 706(1-2):85–110.

Gandolfi, S., Illarionov, A. Y., Fantoni, S., Miller, J., Pederiva, F., and Schmidt, K. (2010). Microscopic calculation of the equation of state of nuclear matter and neutron star structure. *Monthly Notices of the Royal Astronomical Society: Letters*, 404(1):L35–L39.

Garg, U. and Colo, G. (2018). The compression-mode giant resonances and nuclear incompressibility. *Progress in Particle and Nuclear Physics*, 101:55–95.

Glendenning, N. K. (2012). *Compact stars: Nuclear physics, particle physics and general relativity*. Springer Science & Business Media.

Greiner, W. and Maruhn, J. A. (1996). *Nuclear models*. Springer.

Hinderer, T. (2008). Tidal Love numbers of neutron stars. *The Astrophysical Journal*, 677(2):1216.

Hinderer, T., Lackey, B. D., Lang, R. N., and Read, J. S. (2010). Tidal deformability of neutron stars with realistic equations of state and their gravitational wave signatures in binary inspiral. *Physical Review D*, 81(12):123016.

Horowitz, C., Brown, E., Kim, Y., Lynch, W., Michaels, R., Ono, A., Piekarewicz, J., Tsang, M., and Wolter, H. (2014). A way forward in the study of the symmetry energy: experiment, theory, and observation. *Journal of Physics G: Nuclear and Particle Physics*, 41(9):093001.

Khoa, D. T. and Satchler, G. (2000). Generalized folding model for elastic and inelastic nucleus–nucleus scattering using realistic density dependent nucleon–nucleon interaction. *Nuclear Physics A*, 668(1-4):3–41.

Khoa, D. T., Satchler, G., and Von Oertzen, W. (1997). Nuclear incompressibility and density dependent NN interactions in the folding model for nucleus-nucleus potentials. *Physical Review C*, 56(2):954.

Khoa, D. T., Von Oertzen, W., Bohlen, H., and Ohkubo, S. (2007). Nuclear rainbow scattering and nucleus–nucleus potential. *Journal of Physics G: Nuclear and Particle Physics*, 34(3):R111.

Khoa, D. T., Von Oertzen, W., and Ogloblin, A. (1996). Study of the equation of state for asymmetric nuclear matter and interaction potential between neutron-rich nuclei using the density-dependent M3Y interaction. *Nuclear Physics A*, 602(1):98–132.

Lattimer, J. M. (2014). Symmetry energy in nuclei and neutron stars. *Nuclear Physics A*, 928:276–295.

Lattimer, J. M. and Prakash, M. (2004). The physics of neutron stars. *science*, 304(5670):536–542.

Le Tiec, A. and Casals, M. (2021). Spinning black holes fall in love. *Physical Review Letters*, 126(13):131102.

Li, B.-A., Chen, L.-W., and Ko, C. M. (2008). Recent progress and new challenges in isospin physics with heavy-ion reactions. *Physics Reports*, 464(4-6):113–281.

Loan, D. T., Tan, N. H., Khoa, D. T., and Margueron, J. (2011). Equation of state of neutron star matter, and the nuclear symmetry energy. *Physical Review C*, 83(6):065809.

Metzger, B. D., Thompson, T. A., and Quataert, E. (2018). A magnetar origin for the kilonova ejecta in GW170817. *The Astrophysical Journal*, 856(2):101.

Moustakidis, C. C. and Panos, C. (2009). Equation of state for β-stable hot nuclear matter. *Physical Review C*, 79(4):045806.

Ono, A., Danielewicz, P., Friedman, W., Lynch, W., and Tsang, M. (2003). Isospin fractionation and isoscaling in dynamical simulations of nuclear collisions. *Physical Review C*, 68(5):051601.

Pani, P., Gualtieri, L., Abdelsalhin, T., and Jiménez-Forteza, X. (2018). Magnetic tidal Love numbers clarified. *Physical Review D*, 98(12):124023.

Perot, L. and Chamel, N. (2021). Role of dense matter in tidal deformations of inspiralling neutron stars and in gravitational waveforms with unified equations of state. *Physical Review C*, 103(2):025801.

Tan, N. H., Khoa, D. T., and Loan, D. T. (2020). Spin-polarized β-stable neutron star matter: The nuclear symmetry energy and GW170817 constraint. *Physical Review C*, 102(4):045809.

Tan, N. H., Khoa, D. T., and Loan, D. T. (2021). Equation of state of asymmetric nuclear matter and the tidal deformability of neutron star. *arXiv preprint arXiv:2104.09121*.

Tan, N. H., Loan, D. T., Khoa, D. T., and Margueron, J. (2016). Mean-field study of hot β-stable protoneutron star matter: Impact of the symmetry energy and nucleon effective mass. *Physical Review C*, 93(3):035806.

Tews, I. and Schwenk, A. (2020). Spin-polarized neutron matter, the maximum mass of neutron stars, and GW170817. *The Astrophysical Journal*, 892(1):14.

Thân, H. S. (2010). *UFR SCIENTIFIQUE D'ORSAY INSTITUT DE PHYSIQUE NUCLEAIRE D'ORSAY*. PhD thesis, Citeseer.

Trippa, L., Colò, G., and Vigezzi, E. (2008). Giant dipole resonance as a quantitative constraint on the symmetry energy. *Physical Review C*, 77(6):061304.

Tsang, M., Chajecki, Z., Coupland, D., Danielewicz, P., Famiano, F., Hodges, R., Kilburn, M., Lu, F., Lynch, W., Winkelbauer, J., et al. (2011). Constraints on the density dependence of the symmetry energy from heavy-ion collisions. *Progress in Particle and Nuclear Physics*, 66(2):400–404.

Vidana, I. and Bombaci, I. (2002). Equation of state and magnetic susceptibility of spin polarized isospin asymmetric nuclear matter. *Physical Review C*, 66(4):045801.

Xie, W.-J. and Li, B.-A. (2019). Bayesian inference of high-density nuclear symmetry energy from radii of canonical neutron stars. *The Astrophysical Journal*, 883(2):174.

Yagi, K. (2014). Multipole love relations. *Physical Review D*, 89(4):043011.

Yagi, K. (2017). Erratum: Multipole love relations [phys. rev. d 89, 043011 (2014)]. *Physical Review D*, 96(12):129904.